Supporting Information

Structural Modulation of Low Valent Iron in LDH Derived Ni_3Se_4 Nanosheets: A Breakthrough Electrocatalyst for overall water splitting reaction

Arun Karmakar,[†‡] Abhirami V Krishnan,[#] Rahul Jayan,[$] Ragunath Madhu,[†‡] Md Mahbubul Islam [$]* and Subrata Kundu [†‡]*

[†]Academy of Scientific and Innovative Research (AcSIR), Ghaziabad-201002, India.

[‡]Electrochemical Process Engineering (EPE) Division, CSIR-Central Electrochemical Research Institute (CECRI), Karaikudi-630003, Tamil Nadu, India.

[#]Department of Chemistry, Wayne State University, Detroit-48201, USA.

[$] Department of Mechanical Engineering, Wayne State University, Detroit-48201, USA.

*To whom correspondence should be addressed, *E-mail: skundu@cecri.res.in; kundu.subrata@gmail.com, gy5553@wayne.edu*. Phone/Fax: (+ 91) 4565-241487.

This file contains 23 pages in which the details of Electrodes fabrications, material preparation for different characterizations, data for OER, comparative electrocatalysis datas are given in detail.

Number of Figure: 12

Number of Table: 2

1. Reagents and Instruments:

Iron chloride [$FeCl_2.6H_2O$], Nickel Nitrate [$Ni(NO_3)_2.6H_2O$], Urea and ammonium fluoride (NH_4F) were were purchased from Sigma-Aldrich and used as received. Sodium hydroxide (NaOH), Selenium powder (Se) and hydrazine (N_2H_4) hydrate was purchased from Merck and used as received. The used carbon cloth as working electrode substrate purchased from Sigma-Aldrich and used after surface cleaning. DI water was used throughout entire experiments. ICP-MS analysis was carried by using iCAP RQ from thermoscientific instrument. The as prepared catalysts like pristine NiFe-LDH and $Fe@Ni_3Se_4$ were characterized with HR-TEM, (Tecnai^{TM} G^2 TF20) working at an accelerating voltage of 200 kV and by Talos F-200-S with HAADF elemental mapping. Energy Dispersive X-ray Spectroscopy (EDS) **analysis** were carried out with the FE-SEM instrument with the images (SUPRA 55VP Carl Zeiss). Scanning Electron Microscopy (SEM) analysis was carried with a Hitachi, Japan make model S-3000H instrument having magnification 30× to 300 k× with the accelerating voltage ~ 0.3 to 30 kV. The XRD analysis carried out with a scanning rate of 5° min^{-1} in the 2θ range 10-90° using a Rigaku X-ray powder diffractometer (XRD) with Cu K_α radiation (λ = 0.154 nm). X-ray photoelectron spectroscopic (XPS) analysis was performed using a Theta Probe AR-XPS system (Thermo-Fisher Scientific, UK).

2. Electrochemical Characterization:

The electrochemical analyzer AURT-M204 has utilized for all electrochemical characterizations. The used Hg/HgO (1 M KOH) electrode used as reference electrode was purchased from CH instrument. The graphite rod was purchased from Alfa Aesar and has used as the counter electrode. Entire potential data that were collected by taking Hg/HgO as a reference electrode and later it was converted to reversal hydrogen electrode (E_{RHE}) scale by considering the Nernst equation of

$$E_{RHE} = E_{ref} + 0.059\times14 + 0.098 \quad \text{S1}$$

Over potential (η) values pristine NiFe-LDH, Fe@Ni_3Se_4 and other catalyst at benchmarking current density of 10, 50 and 100 mA/cm^2 is calculated by following this equation[1]

$$\eta = E_{RHE} - 1.23 \text{ V (for OER)} \quad \text{S2}$$

$$\eta = 0 - E_{RHE} \text{ (for HER)} \quad \text{S3}$$

Tafel slope was calculated from 100 % iR-drop free LSV polarization data followed by fitting η *vs* log (current density) using the Tafel equation

$$\eta = \beta \cdot \log(j/j_0) \quad \text{S4}$$

where β signify the Tafel slope value, j signifies the current density and j_0 is the exchange current density. Electrochemical impedance spectroscopy (EIS) measurements were done on the frequency ranges from 10^5 to 1 Hz at 150 mV *vs* RHE for HER. In addition, the Operando-EIS study has done by using modified GC electrode as working electrode at different applied potential. The value of electrochemical active surface areas (ECSA) can be measured by determining the electrochemical double layer capacitance (C_{dl}) as follows:

$$\Delta J = \nu \times C_{dl} \quad \text{S5}$$

$$\text{ECSA} = \frac{C_{dl}}{C_s} \quad \text{S6}$$

where ΔJ designates the double-layer charging current resulting from scan-rates (ν) dependent CV outcomes at non-faradic potential region, C_s denotes a specific capacitance value of 0.040 mF/cm^2 depending on the typical reported values. The specific activity of the catalysts was determined by normalizing the geometrically normalized current density with respect to electrochemical active surface area (ECSA) values i.e.,

$$J_{ECSA} = \frac{J_{geo}}{ECSA} \quad \text{S7}$$

3. Synthesis of NiFe-LDH@NF:

Prior to synthesis, a piece of 5 × 3 cm Ni foam (NF) was dipped in diluted hydrochloric acid to remove oxide coatings on the surface, then sonicated for 5 minutes before being washed with ethanol and deionized water numerous times respectively. Typically, the synthesis of NiFe-LDH@NF: 0.01 M $Ni(NO_3)_2.6H_2O$, 0.01 M $FeCl_2.4H_2O$,0.05 M $CO(NH_2)_2$ and NH_4F were dissolved in 1:1 mixture of 15ml of deionized water and 15ml of ethanol with stirring for 10 minutes. The resulting solution was subsequently transferred into a 100ml Teflon-lined stainless-steel autoclave, and the as-prepared NF was immersed into the solution. The hydrothermal reaction was carried out at 160℃ in an electric oven for 12 hours and thereafter cooled down to room temperature. After the reaction, the NiFe-LDH sample coated on NF was collected, washed by deionised water for several times and then dried overnight. Also, the suspension was centrifugated, washed with DI water and ethanol respectively and dried at 50℃, and then NiFe-LDH was obtained.

4. **Synthesis of Fe@Ni_3Se_4:**

15 mmol of Se powder and 1 bead of NaOH was dispersed in DMF/N2H4 mixture (35 ml and 0.6 ml respectively) and stirred for about 10 min. Thereafter the resultant solution was transferred into an autoclave with the as-prepared NiFe-LDH@NF leaning against the wall and kept at 160℃ for 20 hours. The selenized nickel foam was taken out from the autoclave and dried once it had cooled down to room temperature. The overall synthetic scheme has been portrayed as Scheme 1.

5. **Determination of Surface concentration of Fe@Ni_3Se_4 from the redox features of CV:**[2]

Calculated area associated with the oxidation of Ni^{3+} to Ni^{4+} = 0.00207 VA

Hence, the associated charge is = 0.00207 VA / 0.1 Vs^{-1}

= 0.0207 As

= 0.0207 C

Now, the number of electron transferred is = 0.0207 C / 1.602 $\times 10^{-19}$ C

$$= 1.29 \times 10^{17} \text{ C}$$

Since, the oxidation of Ni^{3+} to Ni^{4+} is a single electron transfer reaction, the number electron calculated above is exactly the same as the number of surface-active sites.

Hence, the number of Ni participate in OER is = 1.29 $\times 10^{17}$ C

Determination of Turnover Frequency (TOF) from OER Current Density TOF in our study was calculated assuming that the surface-active Ni atoms that had undergone the redox reaction just before onset of OER only participated in OER electrocatalysis. The corresponding expression is,

$$TOF = \frac{j \times N_A}{F \times n \times \tau} \ldots\ldots\ldots \text{S8}$$

Where, j = current density, N_A= Avogadro number, F = Faraday constant, n = Number of electrons and τ = Surface concentration.

Hence, we have,

$$TOF_{1.55\,V} = \frac{(137 \times 10^{-3}) \times (6.023 \times 10^{23})}{(96485) \times (4) \times (1.29 \times 10^{17})} = 1.6631 \text{ sec}^{-1}$$

Similarly, the TOF values for pristine NiFe-LDH and Ni_3Se_4 were calculated form the redox feature and calculated values are 0.96 and 0.50 sec^{-1}.

6. DFT calculation parameters

For all the spin polarized DFT computations, we used the Vienna Ab initio Simulation software (VASP).[3] To probe the electron-electron exchange correlations, we used the projected augmented wave (PAW) method and the Perdew-Bruke-Ernzerhof (PBE) functional within the framework of generalized gradient approximations. The van der Waal (vdW) interactions between the substrates were accounted using Grimme's DFT-D2 approach. The calculations in the plane-wave (PW) basis were performed with a kinetic cutoff energy of 500 eV. To explore the atom and cell parameter positions, we used the conjugate gradient approach. The self-consistent calculation convergence conditions were set at 10^{-4}

eV/in energy and 10^{-2} eV/in force. By introducing 20 Å vacuum gap along the z direction, the interaction between the two neighboring images was avoided. The Monkhorst-Pack method was used to create k-point meshes of 5×5×1 and 11×11×1 to sample the Brillouin zone for both structural and electronic relaxations. The interfacial charge transfer between the substrates was calculated using Bader charge analysis.

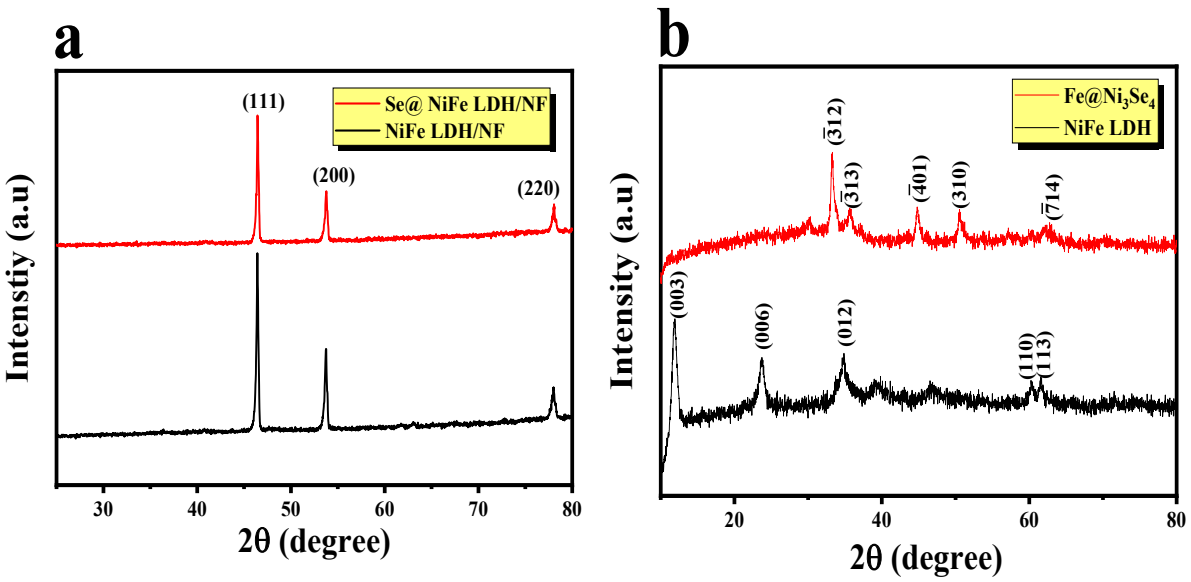

Figure S1: *(a) XRD spectrum of pristine NiFe-LDH and Fe@Ni_3Se_4 materials over nickel foam and (b) XRD features of pristine NiFe-LDH and Fe@Ni_3Se_4 materials powder materials.*

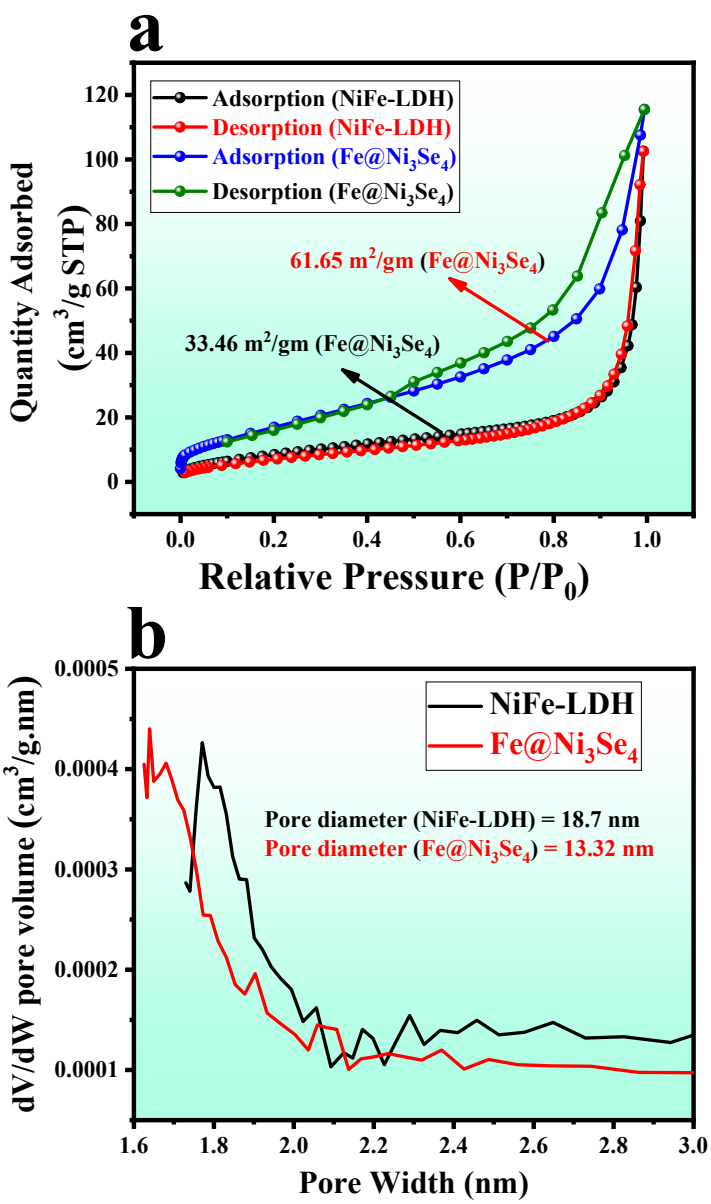

Figure S2: *(a) Brunauer–Emmett–Teller (BET), N_2 adsorption-desorption isotherm for pristine NiFe-LDH and Fe@Ni_3Se_4 and (b) BJH pore size distribution profile.*

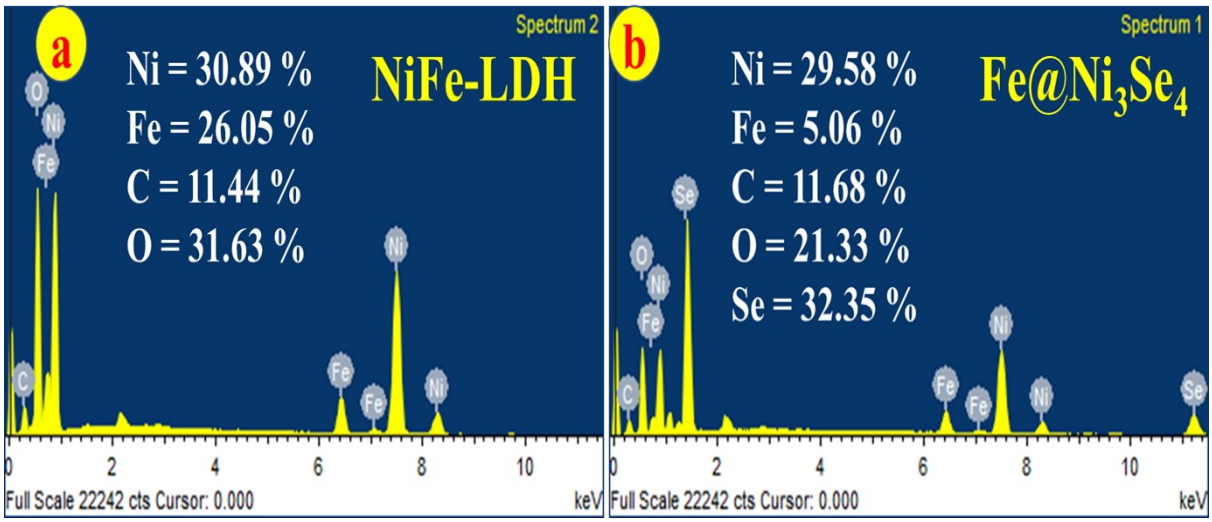

Figure S3: *(a) EDS spectrum of NiFe-LDH with corresponding quantification of various elements like Ni. Fe, C and O; (b) EDS spectrum of NiFe-LDH with corresponding quantification of various elements like Ni. Fe, C, Se and O.*

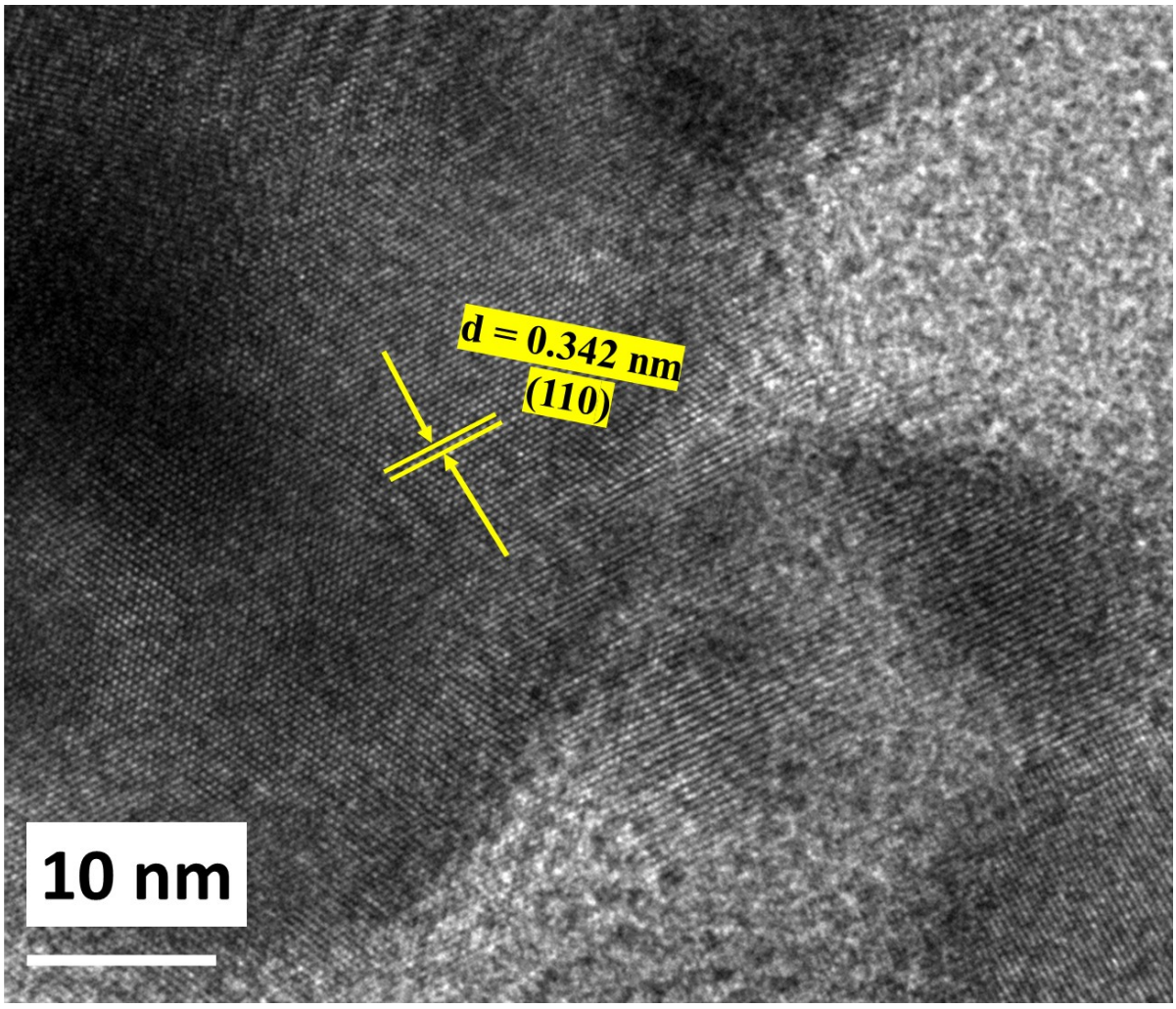

Figure S3: *(a) EDS spectrum of NiFe-LDH with corresponding quantification of various elements like Ni. Fe, C and O; (b) EDS spectrum of NiFe-LDH with corresponding quantification of various elements like Ni. Fe, C, Se and O.*

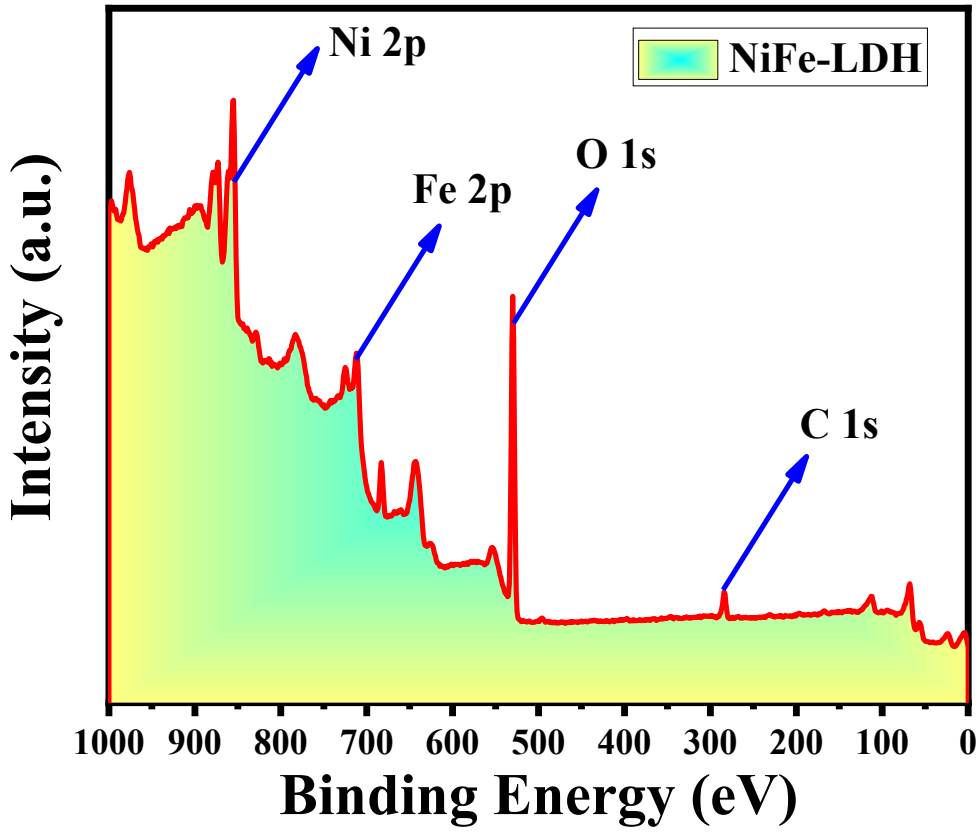

Figure S4: *XPS-survey spectrum of pristine NiFe-LDH materials representing the presence of various elements like Ni, Fe, C and O.*

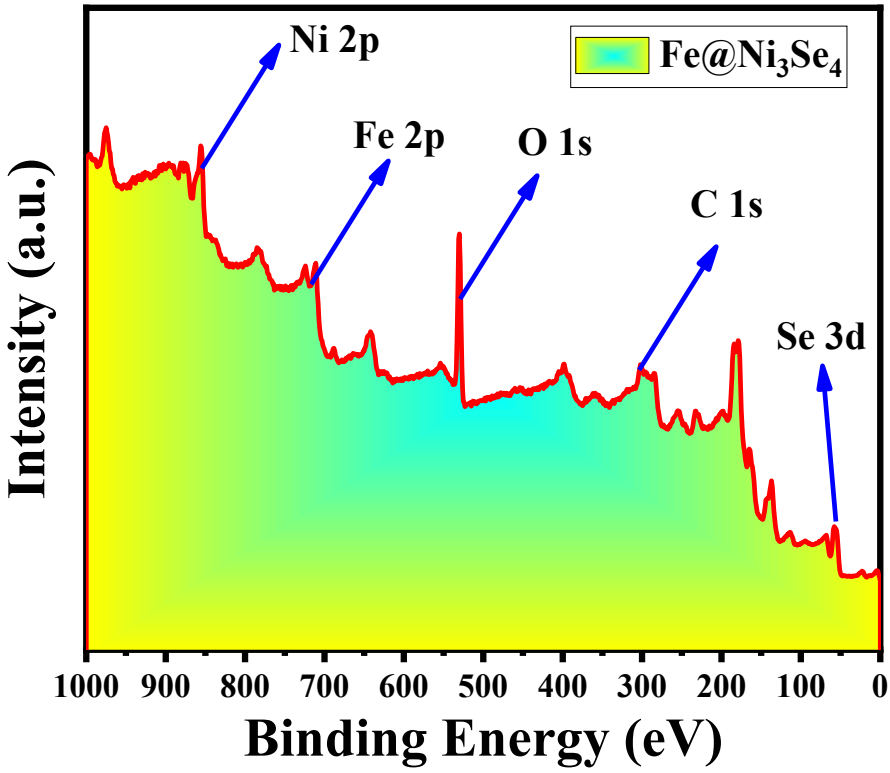

Figure S5: *XPS-survey spectrum of pristine Fe@Ni_3Se_4 materials representing the presence of various elements like Ni, Fe, C and O.*

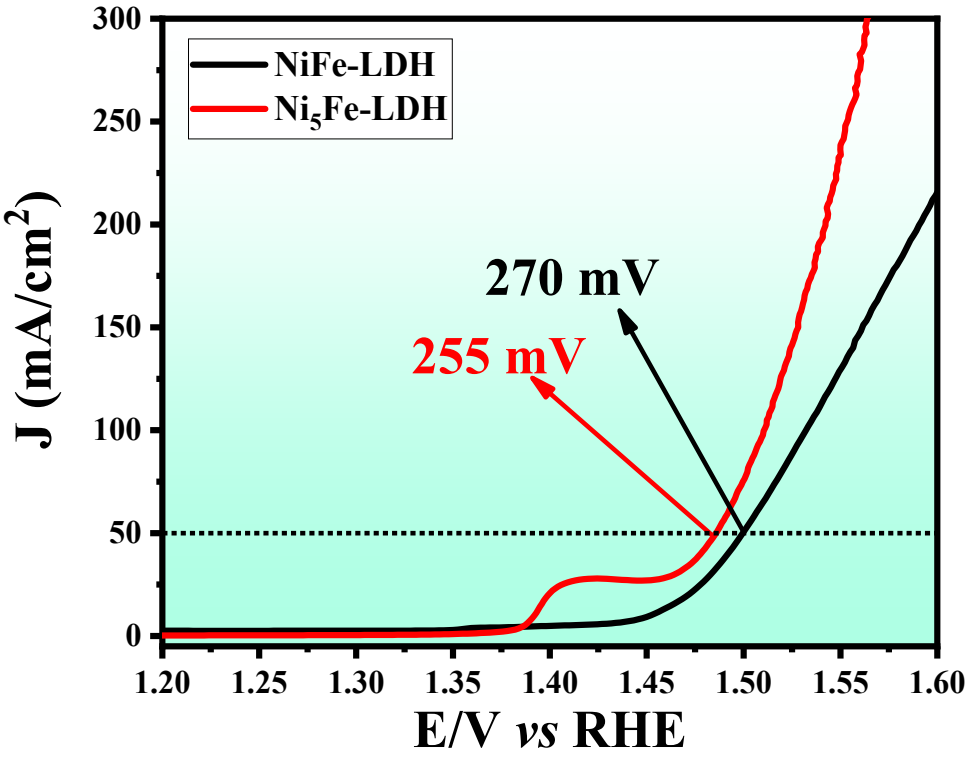

Figure S6: *Linear sweep voltametric outcomes of NiFe-LDH and Ni5Fe-LDH materials in 1 M KOH acquired with a scan rate of 5 mV/sec.*

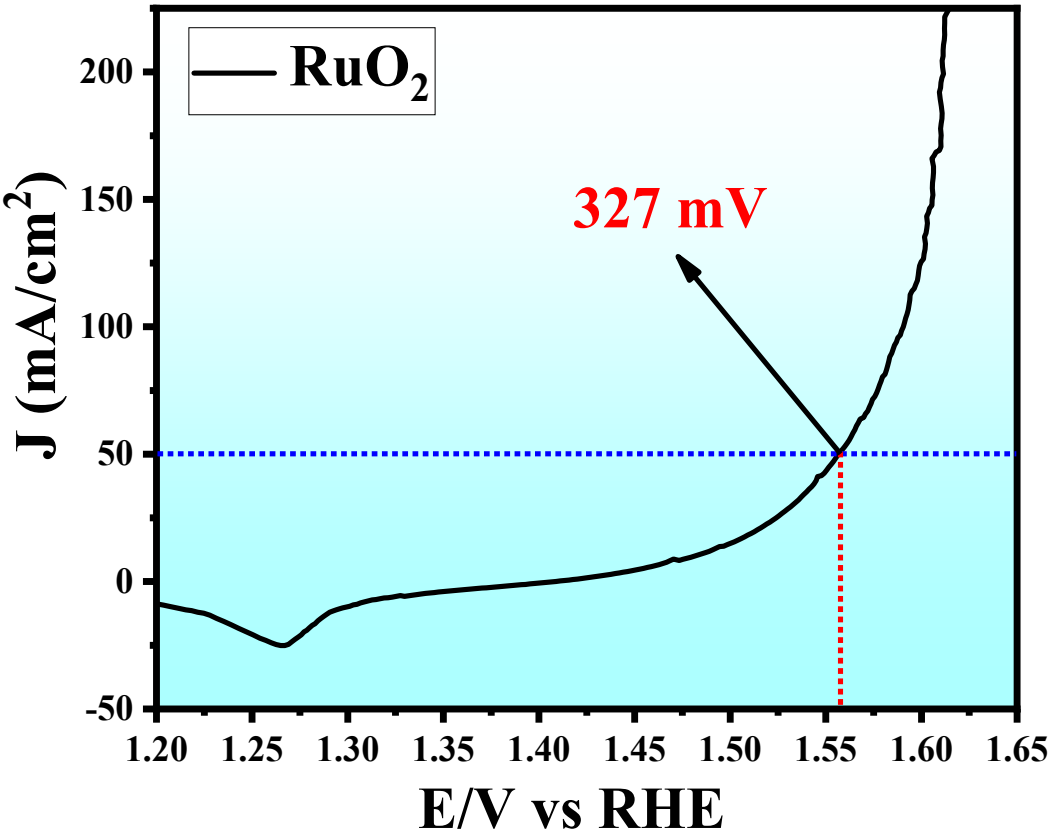

Figure S7: *Linear sweep voltametric outcomes of commercial RuO_2 material acquired with a scan rate of 5 mV/sec in 1 M KOH solution.*

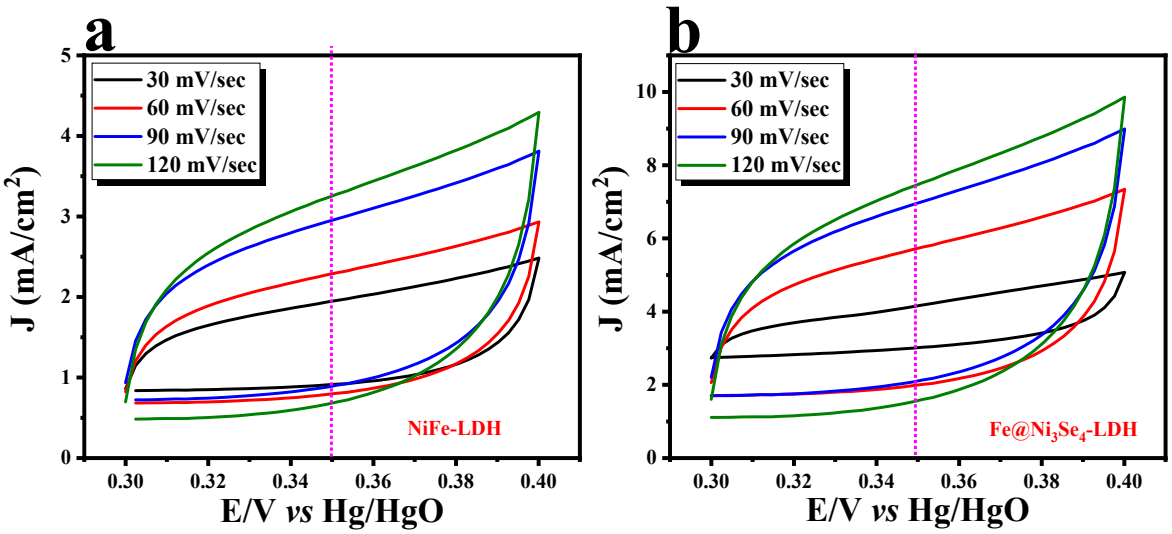

Figure S8: *Cyclic voltammetry feature of (a) pristine NiFe-LDH and (b) Fe@Ni_3Se_4 with a different applied scan rate value for obtaining the C_{dl} information.*

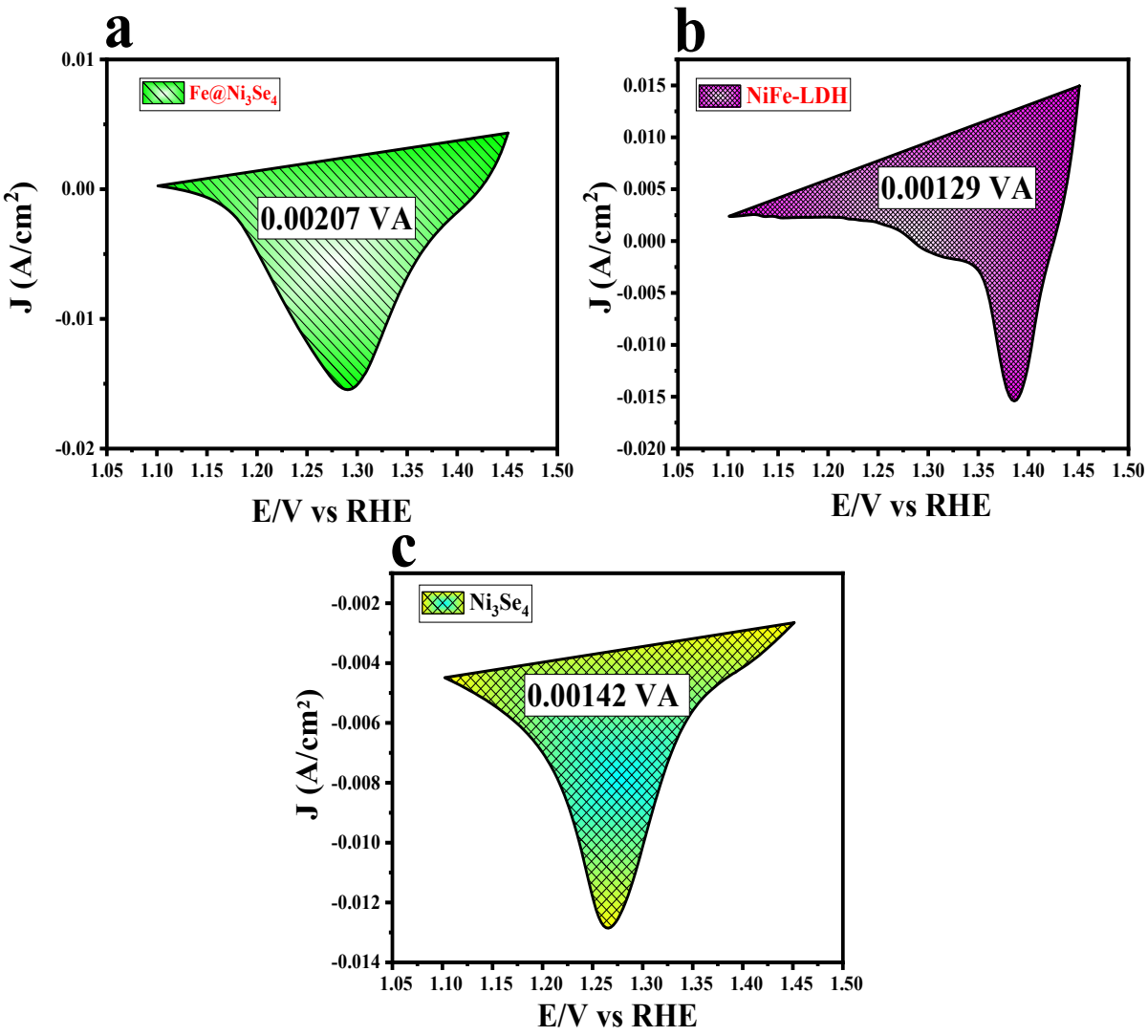

Figure S9: *Reduction area corresponding to Ni^{4+} to Ni^{3+} conversion of (a) $Fe@Ni_3Se_4$; (b) pristine NiFe-LDH and (c) Ni_3Se_4 materials.*

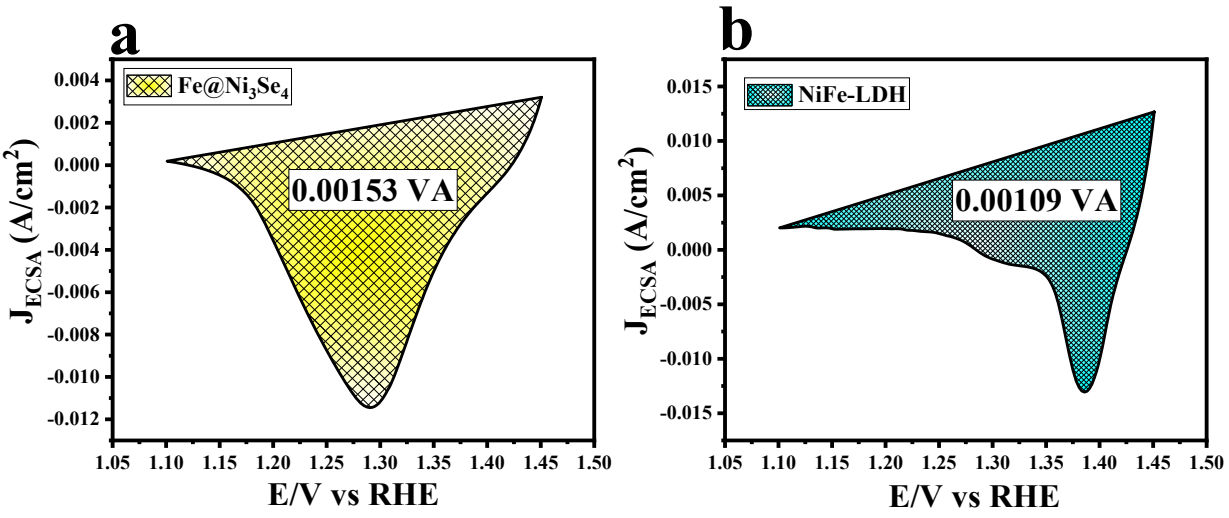

Figure S10: *ECSA normalized Reduction area corresponding to Ni^{4+} to Ni^{3+} conversion of (a) $Fe@Ni_3Se_4$ and (b) pristine NiFe-LDH materials.*

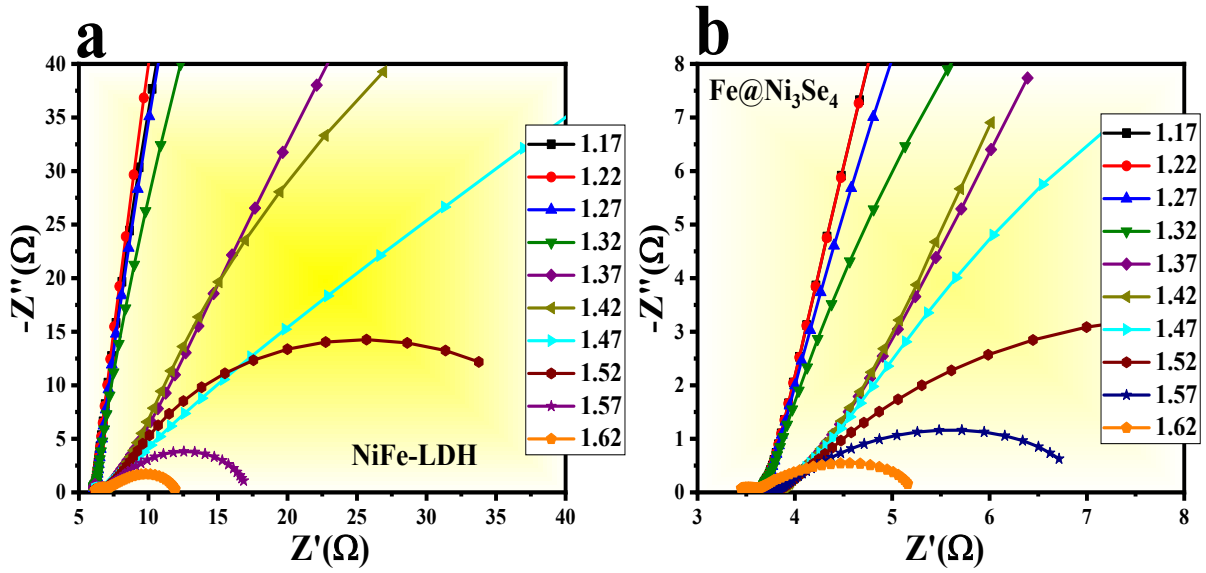

Figure S11: *Nyquist plot for (a) pristine NiFe-LDH and (b) Fe@Ni_3Se_4 at different applied potential.*

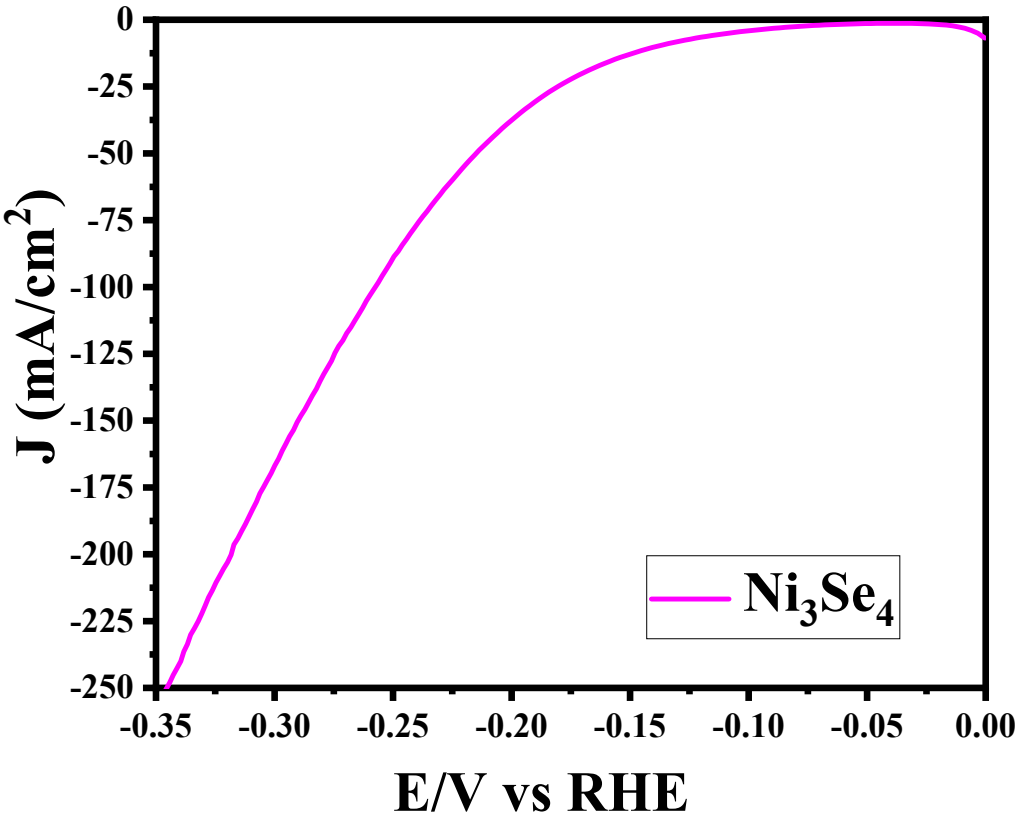

Figure S12: HER, LSV polarization information of pristine Ni_3Se_4 in alkaline condition.

Table S1: Comparison table for comparing the electrochemical OER performance of $Fe@Ni_3Se_4$ with similar types of catalyst reported recently.

Electrocatalyst	**Overpotential η_{OER} (mV)**	**Current density j (mA cm^{-2})**	**Electrolyte**	**Tafel**	**Stability (h)**	**Ref**
NiFe LDH/NF	222 mV	100 mA cm^{-2}	1 M KOH	42.3mV dec^{-1}	20 h	4
NiFeCo-LDH/CF	249 mV	10 mA cm^{-2}	1M KOH	42 mV dec^{-1}	20 h	5
3D NiFeLDH HMS	290 mV	10 mA cm^{-2}	1 M KOH	51 mV dec^{-1}	-	6
NiFe-LDH@NiFe-Bi/CC	294 mV	50 mA cm^{-2}	1 M KOH	96 mV dec^{-1}	20 h	7
NiFe LDH/NiTe	228 mV	50 mA cm^{-2}	1 M KOH	51.04 mV dec^{-1}	30 h	8
Exf NiFe LDH/CB	220 mV	10 mA cm^{-2}	1 M KOH	35 mV dec^{-1}	12 h	9
PLDH/0.1GO	236 mV	10 mA cm^{-2}	1 M KOH	52 mV dec^{-1}	13 h	10
NiFe LDH/CuO NS	270 mV	20 mA cm^{-2}	1 M KOH	34.7 mV dec^{-1}	-	11
NiFe2O4/NiFeLDH-25/SSM	190 mV	100 mA cm^{-2}	1 M KOH	21.5 mV dec^{-1}	6 h	12
Ta-NiFe LDH	260 mV	50 mA cm^{-2}	1 M KOH	58.95 mV dec^{-1}	20 h	13
NiFe LDH/NiCoP@NC	210 mV	10 mA cm^{-2}	1 M KOH	35 mV dec^{-1}	30 h	14
NiFe-$V_{1.0}$ LDH	254 mV	10 mA cm^{-2}	1 M KOH	43.37 mV dec^{-1}	20 h	15
$NiCo_2S_4$@NiFe LDH	287 mV	10 mA cm^{-2}	0.1 M KOH	86.4 mV dec^{-1}	10 h	16
(Co,Ni)Se_2@NiFe LDH	277 mV	10 mA cm^{-2}	1 M KOH	75 mV dec^{-1}	17 h	17
NiFe LDH@CoP/NiP_3	300 mV	82 mA cm^{-2}	1 M KOH	94 mV dec^{-1}	70 h	18
$Fe@Ni_3Se_4$	**201 mV**	**50 mA cm^{-2}**	**1 M KOH**	**40 mV dec^{-1}**	**50 h**	**This work**

Table S2: Comparison table for comparing the electrochemical HER performance of $Fe@Ni_3Se_4$ with similar types of catalyst reported recently.

Electrocatalyst	Overpotential η_{HER} (mV)	Current density j (mA cm^{-2})	Electrolyte	Tafel	Stability (h)	Ref
NiFeAu LDH	89 mV	10 mA cm^{-2}	1 M KOH	90 mV dec^{-1}	30 h	19
NiFeIr LDH	77 mV	100 mA cm^{-2}	1 M KOH	32 mV dec^{-1}	22 h	20
CoNiN@NiFe LDH	150 mV	10 mA cm^{-2}	1 M KOH	169 mV dec^{-1}	50 h	21
$NiFeIr^{3+}$-LDH	19 mV	10 mA cm^{-2}	1 M KOH	37.5 mV dec^{-1}	80 h	22
NF@NiFe LDH/CeOx,	154 mV	10 mA cm^{-2}	1 M KOH	101 mV dec^{-1}	20 h	23
Pt/NiFe-ED	81 mV	100 mA cm^{-2}	1 M KOH	45 mV dec^{-1}	24 h	24
ZCS@NFL/NF	110 mV	10 mA cm^{-2}	1 M KOH	94.9 mV dec^{-1}	48 h	25
Ru-doped $NiFe_2O_4$	18 mV	10 mA cm^{-2}	1 M KOH	27 mV dec^{-1}	38 h	26
Ni/NiFe-LDO/NF	29 mV	10 mA cm^{-2}	1 M KOH	82 mV dec^{-1}	24 h	27
NiFeSP/NF	70 mV	10 mA cm^{-2}	1 M KOH	69 mV dec^{-1}	10 h	28
$Ni_{0.8}Fe_{0.2}Se_2$/CFC	64 mV	10 mA cm^{-2}	0.5 M H_2SO_4	43 mV dec^{-1}	-	29
NiFe LDH/GC	116 mV	10 mA cm^{-2}	1 M KOH	74 mV dec^{-1}	12 h	30
NiFe LDH@NiCoP/NF	120 mV	10 mA cm^{-2}	1 M KOH	88.2 mV dec^{-1}	100 h	31
GDY NiFe LDH/CF	163 mV	10 mA cm^{-2}	1 M KOH	106 mV dec^{-1}	10 h	32
$NiFe_2O_4$/NiFe LDH/NF	101 mV	10 mA cm^{-2}	1 M KOH	67.1 mV dec^{-1}	20 h	33

$Fe@Ni_3Se_4$	**33 mV**	**10 mA cm^{-2}**	**1 M KOH**	**76 mV dec^{-1}**	**50 h**	**This work**

S. No.	Materials Name	Overpotential (mV)	Tafel slope (mV/dec)	Ref
1	$CoFeN_x$ HNAs/NF	260@50 mA/cm^2	57.6	34
2	Ni_3FeN nanosheets	223@10 mA/cm^2	40	35
3	PA-NiO	310@10 mA/cm^2	36	36
4	Ni_3FeN Nanoparticles	280@10 mA/cm^2	46	37
5	$CoSe_2$@CoNi LDH HNA	250@10 mA/cm^2	55	38
6	NiFe-MMO/CNT	>250@10 mA/cm^2	45	39
7	FeNi-O	213@10 mA/cm^2	32	40
8	Mono-NiTi-MMO	320@10 mA/cm^2	52	41
9	$(Co,Ni)Se_2$@NiFe-LDH	277@10 mA/cm^2	75	17
10	b-$Ni(OH)_2$/NGr	311@10 mA/cm^2	96	42
11	$Ni_{0.8}Fe_{0.2}$-m/t-$Se_{0.02}$-LDH	243@10 mA/cm^2	67	43
12	$Co_{1-x}Fe_xSe_2$ (x = 0.6)	217@10 mA/cm^2	41	44
13	$Fe@Ni_3Se_4$	185@10 mA/cm^2	38	This work

Table S3: Comparison table for comparing the electrochemical OER performance of $Fe@Ni_3Se_4$ with various state-of-art LDH derived materials.

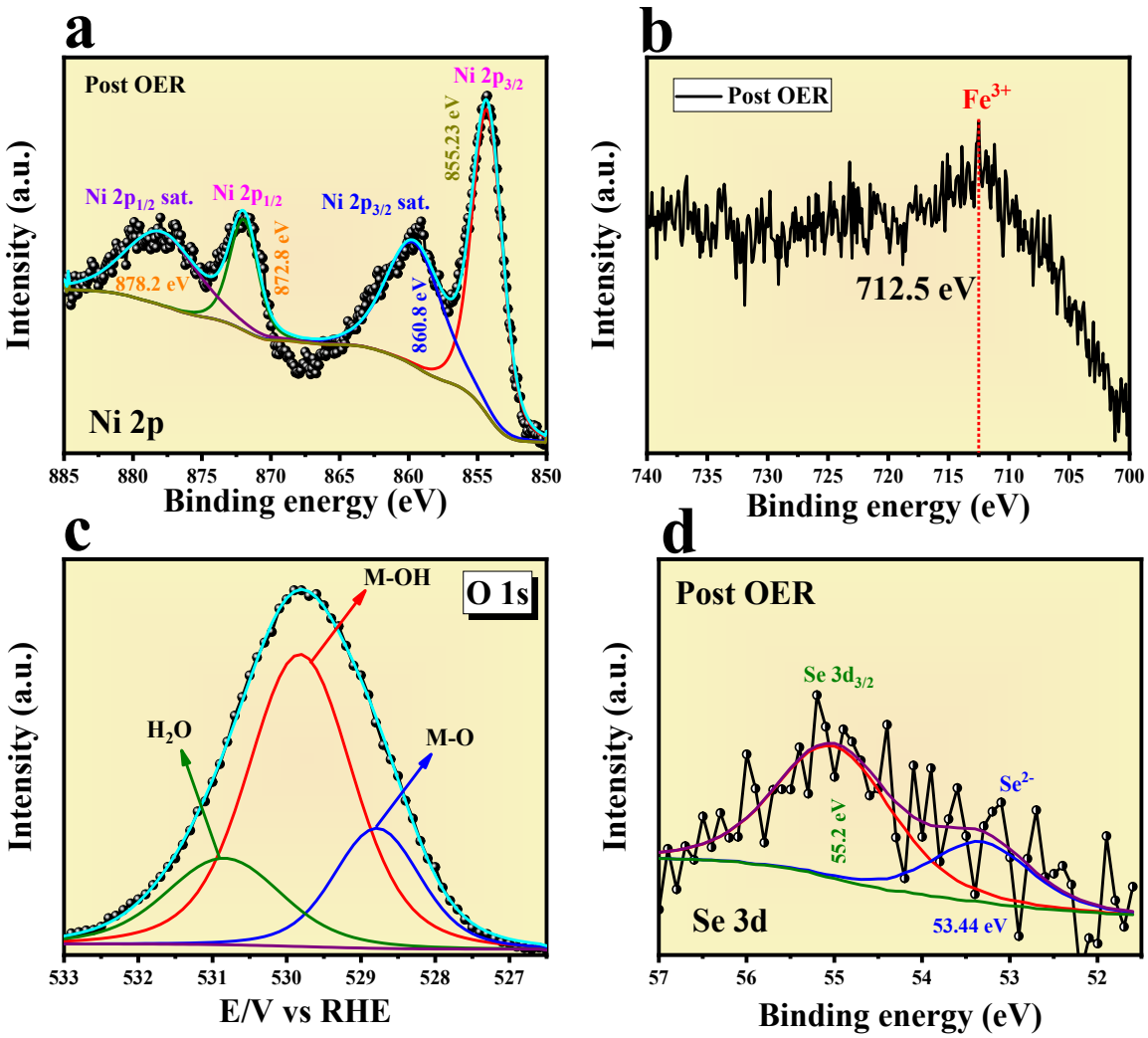

Figure S13: ***(a)*** *deconvoluted XPS spectrum of Ni 2p orbital after long term OER study; (b) deconvoluted XPS spectrum of Fe 2p orbital; (c) and (d) corresponding XPS spectrum for O 1s and Se 3d orbital respectively.*

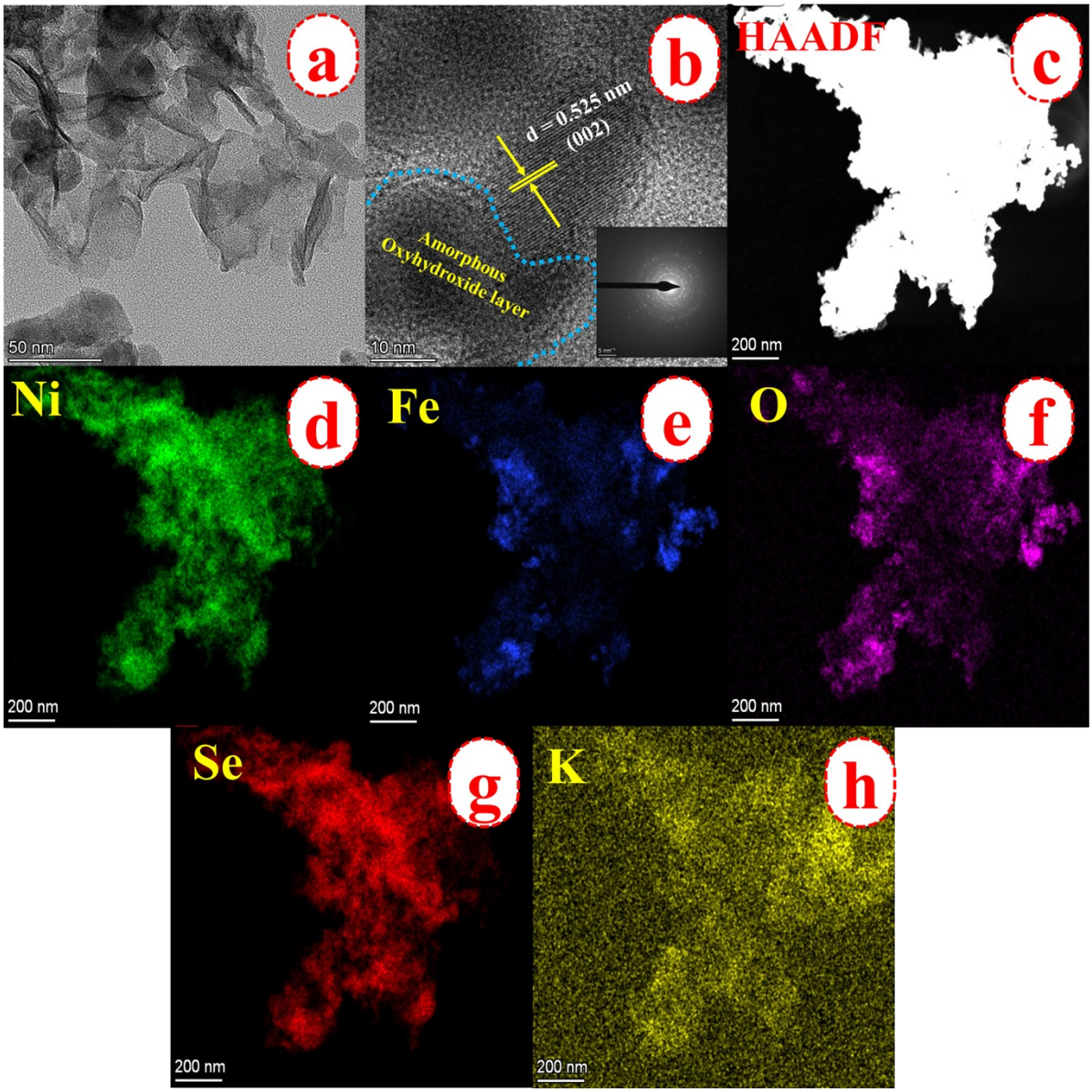

Figure S14: *(a) TEM image of $Fe@Ni_3Se_4$ after OER study; (b) High-resolution TEM image for $Fe@Ni_3Se_4$; inset images portrays SAED pattern which reveals the polycrystalline nature of the particles; (c) shows the selected HADDF area for colour mapping analysis and (d-h) displays corresponding colour mapping result of Ni, Fe, O, Se and K ions respectively.*

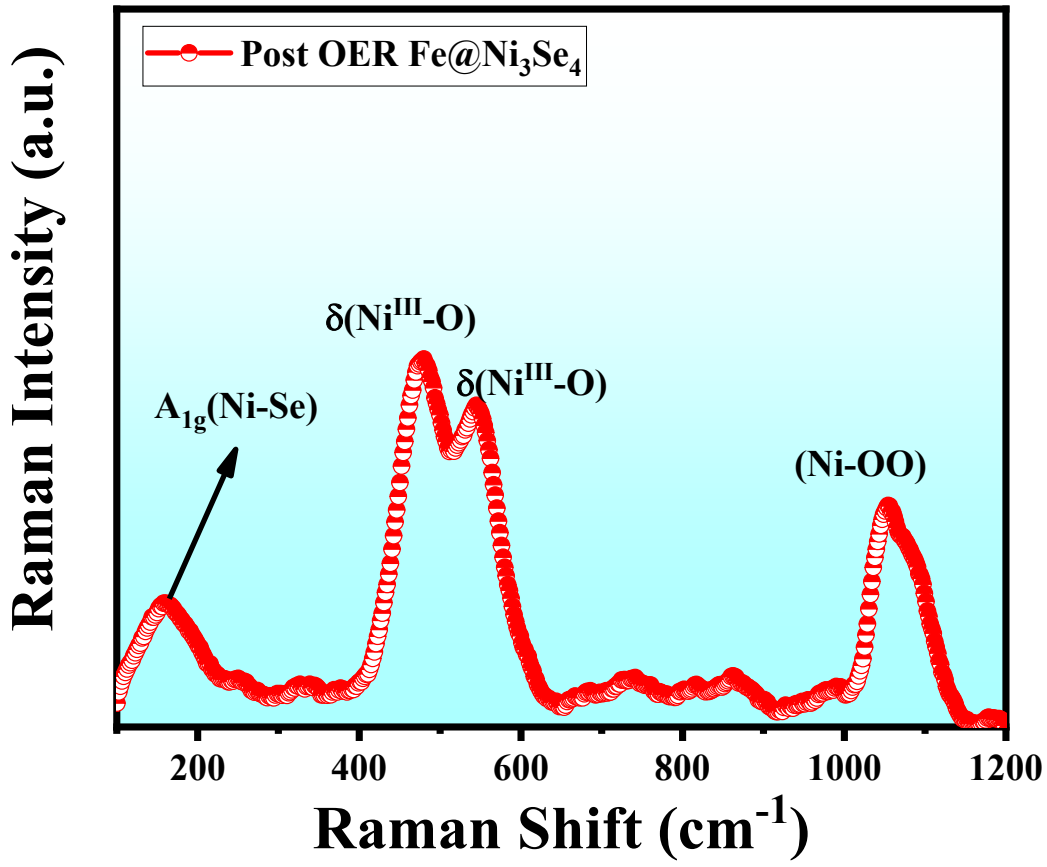

Figure S15: ***(a-b)*** *The optimized structural configuration of Fe doped on octahedral and tetrahedral sites of* Ni_3Se_4.

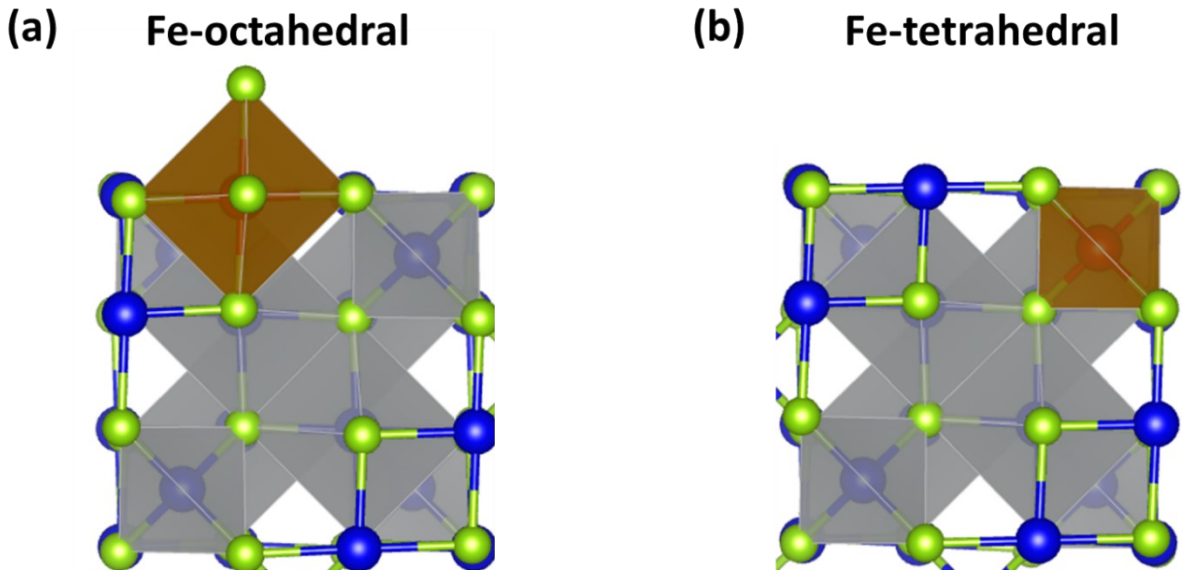

Figure S16: ***(a-b)*** *The optimized structural configuration of Fe doped on octahedral and tetrahedral sites of* Ni_3Se_4.

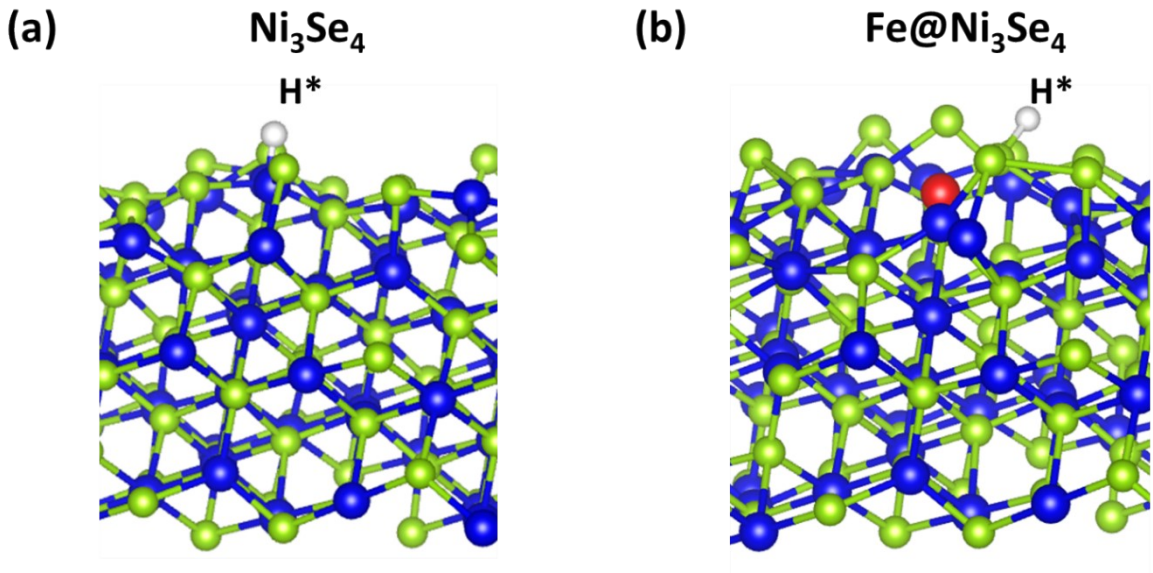

Figure S17: *(a-b) The most stable configuration of H* adsorbed pristine and Fe@Ni_3Se_4 substrate.*

References

1 S. Anantharaj, S. R. Ede, K. Karthick, S. Sam Sankar, K. Sangeetha, P. E. Karthik and S. Kundu, *Energy Environ. Sci.*, 2018, **11**, 744–771.

2 S. Anantharaj, P. E. Karthik and S. Noda, *Angew. Chemie - Int. Ed.*, 2021, **60**, 23051–23067.

3 R. A. Vargas-Hernández, *J. Phys. Chem. A*, 2020, **124**, 4053–4061.

4 H. Yang, C. Wang, Y. Zhang and Q. Wang, *Sci. China Mater.*, 2019, **62**, 681–689.

5 Y. Lin, H. Wang, C. K. Peng, L. Bu, C. L. Chiang, K. Tian, Y. Zhao, J. Zhao, Y. G. Lin, J. M. Lee and L. Gao, *Small*, , DOI:10.1002/smll.202002426.

6 H. Zhong, T. Liu, S. Zhang, D. Li, P. Tang, N. Alonso-Vante and Y. Feng, *J. Energy Chem.*, 2019, **0**, 130–137.

7 L. Zhang, R. Zhang, R. Ge, X. Ren, S. Hao, F. Xie, F. Qu, Z. Liu, G. Du, A. M. Asiri, B. Zheng and X. Sun, *Chem. - A Eur. J.*, 2017, **23**, 11499–11503.

8 L. Hu, X. Zeng, X. Wei, H. Wang, Y. Wu, W. Gu, L. Shi and C. Zhu, *Appl. Catal. B Environ.*, 2020, **273**, 1–7.

9 T. S. Munonde, H. Zheng and P. N. Nomngongo, *Ultrason. Sonochem.*, 2019, **59**, 104716.

10 J. Xie, C. Li, J. Niu, S. Zhang, X. Ou, P. Feng and H. Garcia, *Mater. Lett.*, 2021, **290**, 129517.

11 B. Lin, H. Le, F. Xu and S. Mu, *RSC Adv.*, 2020, **10**, 27424–27427.

12 A. A. Kashale, C. H. Yi, K. Y. Cheng, J. S. Guo, Y. H. Pan and I. W. P. Chen, *ACS Appl. Energy Mater.*, 2020, **3**, 10831–10840.

13 X. Wang, Y. Tuo, Y. Zhou, D. Wang, S. Wang and J. Zhang, *Chem. Eng. J.*, 2021, **403**, 126297.

14 J. Nie, M. Hong, X. Zhang, J. Huang, Q. Meng, C. Du and J. Chen, *Dalt. Trans.*, 2020, **49**, 4896–4903.

15 Y. Kong, Y. Wang, W. Chu and Z. Liu, *J. Alloys Compd.*, 2021, **885**, 160929.

16 X. Feng, Q. Jiao, W. Chen, Y. Dang, Z. Dai, S. L. Suib, J. Zhang, Y. Zhao, H. Li and C. Feng, *Appl. Catal. B Environ.*, 2021, **286**, 119869.

17 J. G. Li, H. Sun, L. Lv, Z. Li, X. Ao, C. Xu, Y. Li and C. Wang, *ACS Appl. Mater. Interfaces*, 2019, **11**, 8106–8114.

18 C. Song, Y. Liu, Y. Wang, S. Tang, W. Li, Q. Li, J. Zeng, L. Chen, H. Peng and Y. Lei,

Sci. China Mater., 2021, **64**, 1662–1670.

19 X. P. Li, W. K. Han, K. Xiao, T. Ouyang, N. Li, F. Peng and Z. Q. Liu, *Catal. Sci. Technol.*, 2020, **10**, 4184–4190.

20 Q. Q. Chen, C. C. Hou, C. J. Wang, X. Yang, R. Shi and Y. Chen, *Chem. Commun.*, 2018, **54**, 6400–6403.

21 J. Wang, G. Lv and C. Wang, *Appl. Surf. Sci.*, 2021, **570**, 151182.

22 M. Wang, J. Q. Wang, C. Xi, C. Q. Cheng, C. G. Kuai, X. L. Zheng, R. Zhang, Y. M. Xie, C. K. Dong, Y. J. Chen and X. W. Du, *Small*, , DOI:10.1002/smll.202100203.

23 X. Wang, Y. Yang, L. Diao, Y. Tang, F. He, E. Liu, C. He, C. Shi, J. Li, J. Sha, S. Ji, P. Zhang, L. Ma and N. Zhao, *ACS Appl. Mater. Interfaces*, 2018, **10**, 35145–35153.

24 Y. Feng, R. Ma, M. Wang, J. Wang, T. Sun, L. Hu, J. Zhu, Y. Tang and J. Wang, *J. Phys. Chem. Lett.*, 2021, **12**, 7221–7228.

25 B. Quan, H. Tong, C. Liu, D. Li, S. Meng, M. Chen, J. Zhu and D. Jiang, *Electrochim. Acta*, , DOI:10.1016/j.electacta.2019.134861.

26 S. Niu, S. Li, J. Hu, Y. Li, Y. Du, X. Han and P. Xu, *Chem. Commun.*, 2019, **55**, 14649–14652.

27 Y. Tian, A. Huang, Z. Wang, M. Wang, Q. Wu, Y. Shen, Q. Zhu, Y. Fu and M. Wen, *Chem. Eng. J.*, 2021, **426**, 131827.

28 Y. Xue and M. Sun, *Int. J. Hydrogen Energy*, 2019, **44**, 16378–16386.

29 T. Wang, D. Gao, W. Xiao, P. Xi, D. Xue and J. Wang, *Nano Res.*, 2018, **11**, 6051–6061.

30 X. Teng, L. Guo, L. Ji, J. Wang, Y. Niu, Z. Hu and Z. Chen, *ACS Appl. Energy Mater.*, 2019, **2**, 5465–5471.

31 H. Zhang, X. Li, A. Hähnel, V. Naumann, C. Lin, S. Azimi, S. L. Schweizer, A. W. Maijenburg and R. B. Wehrspohn, *Adv. Funct. Mater.*, , DOI:10.1002/adfm.201706847.

32 H. Y. Si, Q. X. Deng, L. C. Chen, L. Wang, X. Y. Liu, W. S. Wu, Y. H. Zhang, J. M.

Zhou and H. L. Zhang, *J. Alloys Compd.*, 2019, **794**, 261–267.

33 Z. Wu, Z. Zou, J. Huang and F. Gao, *ACS Appl. Mater. Interfaces*, 2018, **10**, 26283–26292.

34 D. Li, Y. Xing, R. Yang, T. Wen, D. Jiang, W. Shi and S. Yuan, *ACS Appl. Mater. Interfaces*, 2020, **12**, 29253–29263.

35 Y. Wang, C. Xie, D. Liu, X. Huang, J. Huo and S. Wang, *ACS Appl. Mater. Interfaces*, 2016, **8**, 18652–18657.

36 Z. Li, W. Niu, L. Zhou and Y. Yang, *ACS Energy Lett.*, 2018, **3**, 892–898.

37 X. Jia, Y. Zhao, G. Chen, L. Shang, R. Shi, X. Kang, G. I. N. Waterhouse, L. Z. Wu, C. H. Tung and T. Zhang, *Adv. Energy Mater.*, 2016, **6**, 1–6.

38 J. Song, Y. Chen, H. Huang, J. Wang, S. C. Huang, Y. F. Liao, A. E. Fetohi, F. Hu, H. yi Chen, L. Li, X. Han, K. M. El-Khatib and S. Peng, *Adv. Sci.*, 2022, **9**, 1–11.

39 Y. Li, H. He, W. Fu, C. Mu, X. Z. Tang, Z. Liu, D. Chi and X. Hu, *Chem. Commun.*, 2016, **52**, 1439–1442.

40 X. Long, Z. Ma, H. Yu, X. Gao, X. Pan, X. Chen, S. Yang and Z. Yi, *J. Mater. Chem. A*, 2016, **4**, 14939–14943.

41 Y. Zhao, X. Jia, G. Chen, L. Shang, G. I. N. Waterhouse, L. Z. Wu, C. H. Tung, D. Ohare and T. Zhang, *J. Am. Chem. Soc.*, 2016, **138**, 6517–6524.

42 A. Nadeema, P. S. Walko, R. N. Devi and S. Kurungot, *ACS Appl. Energy Mater.*, 2018, **1**, 5500–5510.

43 S. Duan, S. Chen, T. Wang, S. Li, J. Liu, J. Liang, H. Xie, J. Han, S. Jiao, R. Cao, H. L. Wang and Q. Li, *Nanoscale*, 2019, **11**, 17376–17383.

44 J. Y. Zhang, L. Lv, Y. Tian, Z. Li, X. Ao, Y. Lan, J. Ji and C. Wang, *ACS Appl. Mater. Interfaces*, 2017, **9**, 33833–33840.